

Malachite green removal from aqueous solutions by MgO_(86%)·Se_(7%)·Te_(7%) nanocomposites

H. Idriss^{a*}, A. I. Alakhras^b, H. M. El Khair^a

^a *Department of Physics, College of Science, Imam Mohammad Ibn Saud Islamic University (IMSIU), P.O.Box 90950, Riyadh 11623, Saudi Arabia*

^b *Department of Chemistry, College of Science, Imam Mohammad Ibn Saud Islamic University (IMSIU), P.O.Box 90950, Riyadh 11623, Saudi Arabia*

In this work, MgO·Se·Te nanocomposites was fabricated and applied as an inexpensive and effective treatment for malachite green. The materials were characterized for morphology, cryptography, surface area using different techniques. In addition, adsorption tests have been performed as a function of contact time, pH, and initial dye concentration to study their impact on the decolorization of malachite green via MgOSeTe nanocomposite. The result verified nanocomposite formation with crystallite size 10.5 nm and a relative surface area of 42.0525 m²/g. Meanwhile, the MgOSeTe nanocomposite was employed for malachite green removal in an aquatic solution. The findings revealed that the maximum adsorption capacity value was 30.67 mg/g. Furthermore, the adsorption was found to follow the Freundlich isotherm models and follow the pseudo-second-order kinetics.

(Received August 1, 2021; Accepted October 21, 2021)

Keywords: Nanocomposites, Malachite green, XRD, BET, SEM, Adsorption

1. Introduction

Water contamination is one of the most significant challenges facing the world due to the industrial revolution, human activities, population increase, and climate change [1]. There are many environmental pollutants, such as pesticides, heavy metals, and organic compounds. Organic and inorganic pigments are contaminants that can arise in wastewater due to industrial activities, including coloring, cosmetics, and textiles [2-3]. The need for color utilization has grown over 1000 tons/year. About 15% of the dye residues resulting from industrial processes are released into waste streams as liquid waste during the dyeing process [4-5]. In addition, most of the dyes used are toxic, and some stains are recognized as highly harmful and carcinogenic to humans [6]. Malachite green (MG) is an organic dye extensively applied in textiles and pesticides in aquatic environments. Moreover, MG is reported to be carcinogenic and poisonous even at a low concentration of 1 mg/L [7]. Therefore, it is imperative to treat water contaminated with dyes. Different processing such as biological, oxidation, and filtration is employed to eliminate stains from polluted water [8].

Various technology such as coagulation, ion exchange, and heat treatment have been investigated for dye treatment in wastewater. Among those technologies, adsorption is considered one of the best methods for treating wastewater due to its high performance, ease of operation, and cheapest [9]. Furthermore, adsorption is one of the most effective methods for removing dyes from polluted water, for example, zeolite, silica, and metal oxides, because of most industrial dyes' chemical and biological stability [10-11]. Recently, nano oxide materials, e.g., TiO₂, Al₂O₃, ZrO₂, ZnO, NiO, and SiO₂, have significantly focused on environmental remediation due to their exceptional feature [12-13]. MnO has been comprehensively examined for the contaminants treatment [14]. Numerous investigations have mainly focused on using MnO nanoparticles in dye removal; however, it is rarely used as a nanocomposite [15]. There is a wide range of nanocomposite materials intended for environmental remediation due to their distinctive and

* Corresponding author: hjoidriss@gmail.com

unique characteristics [16]. In this article, using heat treatment, MgOSeTe nanocomposite was fabricated and utilized as fast-absorbing materials to eliminate malachite green in the aquatic phase.

2. Materials and method

2.1. Production of MgO.Se.Te nanopowder

MgCO₃ was purchased from Sigma Aldrich and employed as a precursor to achieving MgO nanoparticles. First, a suitable weight of MgCO₃ was put into a ceramic crucible inside the oven under ambient circumstances for thermal decomposition at 700 °C for 6 hours; afterward, the MgO nanoparticle was taken. Next, 1.5g of MgO nanopowder, and 0.125 g of Se powder, and 0.125g of Te powder were put together in a mortar and mixed well to obtain a composite of MgO_(86%).Se_(7%).Te_(7%).

2.2. Characterization of MgO nanopowder

The crystal structure, morphology, surface area and chemical bonding of MgO.Se.Te composite were characterized by X-ray diffraction (XRD), scanning electron microscopy, N₂ adsorption-desorption isotherms respectively.

2.3. Adsorption equilibrium test

The stock solution of MG dye(500 ppm) was made using purified water and kept in the dark place at 25 °C. First; the adsorption equilibrium was accomplished in a 50 ml measuring flask comprising 0.07 g of MgOSeTe nanocomposite. Afterward, 18 ml of MG at different concentrations of 50 to 500 ppm was added to 0.07 g of MgOSeTe and then stirred with the assist of a shaker (250 rpm) for 30 minutes and keeping the pH constant. Next, the beaker's contents were isolated using filter paper (3000 rpm). After the test finished, the solution was extracted from the adsorbent using filter paper and measured using the UV - Vis spectrophotometer. Finally, the volume of MG adsorbed by an adsorbent at a time (t) was estimated using equation(1).

$$q_t = \frac{V(C_0 - C_t)}{m} \quad (1)$$

where, q_t (mg g⁻¹) is mass of dye adsorbed by a unit mass of nanopowder m (g) at time t (min), V is the solution volume (L), C_0 concentration of the dye initially preset and C_t is that at t time in (mg L⁻¹). On the other hand, the removal percentage (%)of the dye by adsorption at time(t) can be calculated by formula (2) [17].

$$removal(\%) = \frac{(C_0 - C_t)}{C_0} \times 100 \quad (2)$$

2.4. Adsorption kinetic test

A mix of MgOSeTe 0.07 g and (18ml) of MG in 50ml beakers with the assist of a shaker (250 rpm) was employed for the kinetic study. The solution was separated from the adsorbent by filter paper at a different time, 10-60 min, and estimated via the UV -Vis spectrophotometer. The quantity of MG adsorbed by an adsorbent at equilibrium (q_e) was calculated by the formula (3) [18].

At equilibrium, an analogous formula is employed to find out the mass adsorbed q_e :

$$q_e = \frac{V(C_0 - C_e)}{m} \quad (3)$$

2.5. Adsorption isotherm theory

In this experiment, Freundlich and Langmuir's isotherm was used to compute the absorption capacity of sorbents.

$$\frac{C_e}{q_e} = \frac{1}{q_m} C_e + \frac{1}{q_m \cdot K_L} \quad \text{Langmuir (linear equation)} \quad (4)$$

$$\ln q_e = \frac{1}{n} \ln C_e + \ln K_F \quad \text{Freundlich linear (equation)} \quad (5)$$

C_e = the equilibrium concentration of adsorbate (mg/L-1) q_e = the amount of dye adsorbed per gram of the adsorbent at equilibrium (mg/g), q_m = maximum monolayer coverage capacity (mg/g) K_L = Langmuir isotherm constant (L/mg). q_m and K_L represent the slope and intercept of C_e/q_e versus C_e plotting. While, k and n of Freundlich formula is obtained of the $\ln q_e$ against $\ln C_e$ chart. K_F and n of the Freundlich model are connected with the adsorptive bond strength and distribution, respectively. To agree with experimental data and kinetic models, the correlation coefficient (R^2) value was applied. Equation (6) represents a pseudo-first-order model having a rate constant k_1 ($\text{L} \cdot \text{min}^{-1}$) [19]. From the slope and intercept of $\ln(q_e - q_t)$ versus t plot, k_1 and q_e can respectively be evaluated.

$$\ln(q_e - q_t) = \ln(q_e) - k_1 \cdot t \quad (6)$$

A pseudo-second-order is modeled by equation (7), where k_2 denotes the rate constant ($\text{g} \cdot \text{mg}^{-1} \cdot \text{min}^{-1}$). Using of t/q_t against t graph, q_e and k_2 are correspondingly obtained from the slope and intercept.

$$\frac{t}{q_t} = \frac{1}{k_2 \cdot q_e^2} + \frac{t}{q_e} \quad (7)$$

3. Result and discussion

3.1. Crystal structure of MgOSeTe

The crystalline structure of the MgO nanocomposite was investigated using X-ray Diffractometer (XRD). The pattern of XRD shows numerous peaks at $2\theta = 36.8^\circ$, 42.8° , 62.3° , 74.5° , and 78.3° corresponding to the (111), (200), (220), (311) and (222) planes of MgO nanoparticle in agreement with the JCPDS card No. 36-1451. Moreover, new peaks at $2\theta = 27.5^\circ$ and 30.1° corresponding to (101) planes of Te and Se in agreement with (COD-9008579) and JCPDS no0 86 -2268) respectively. The top peak area (2θ) of MgO nanocomposite was recorded at 42.8° . Hence, the diffraction peaks can be listed to the face-centered cubic structure of MgO, as shown in fig (1). The expanded lines in the XRD pattern indicated nanoparticles size in the samples. Since the XRD pattern achieves the average crystallite size using Debye - Scherer's equation(8) [20].

$$D = \frac{0.9\lambda}{\beta \cos \theta} \quad (8)$$

where: D , λ , β and θ are the crystallite size, wavelength of the X-ray source ($\text{Cu K}\alpha$), full width at half-maximum (FWHM) and Bragg's diffraction angle respectively [25]. From the equation the the average crystallite size was found to be (10.25 nm).

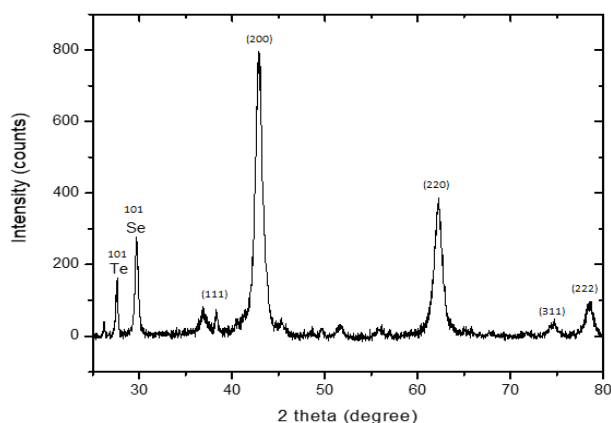


Fig. 1. XRD pattern of MgOSeTe nanocomposite

3.2. Morphology study of MgOSeTe

The morphological investigation of MgOSeTe nanocomposite at various magnifications is illustrated in Fig (2). The images exhibit that MgOSeTe nanocomposite have undifferentiated forms. Generally, the shape of MgOSeTe nanocomposite looks more like cotton flowers. Elemental (EDEX) analysis shows the configuration of MgOSeTe as provided via the elemental ratios.

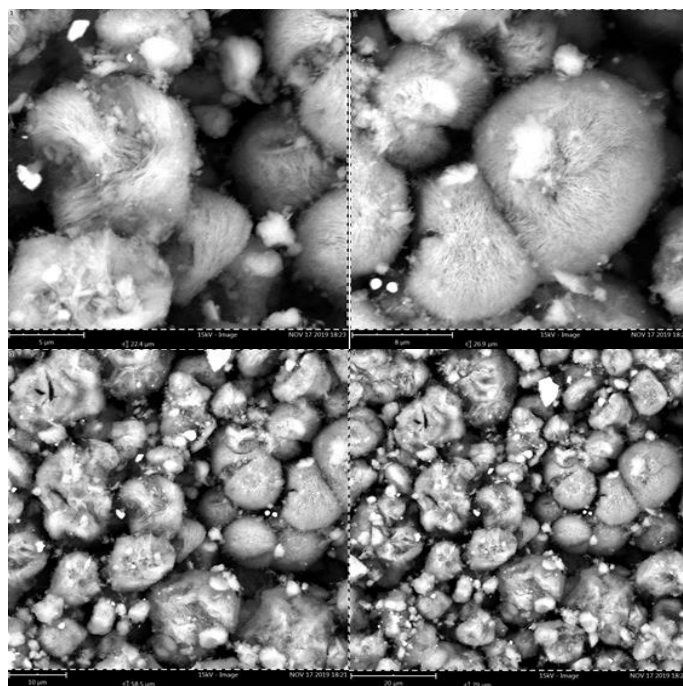


Fig. 2: Morphological images of MgOSeTe nanocomposite.

3.3. Nitrogen Adsorption Study

Nitrogen adsorption-desorption isotherms and the pore size distribution of the MgOSeTe nanocomposite are presented in fig (3). The isotherms demonstrate a type IV with H2 hysteresis loops, which is a feature of mesoporous materials. The summary report of nitrogen adsorption data for MgOSeTe is given in Table 1.

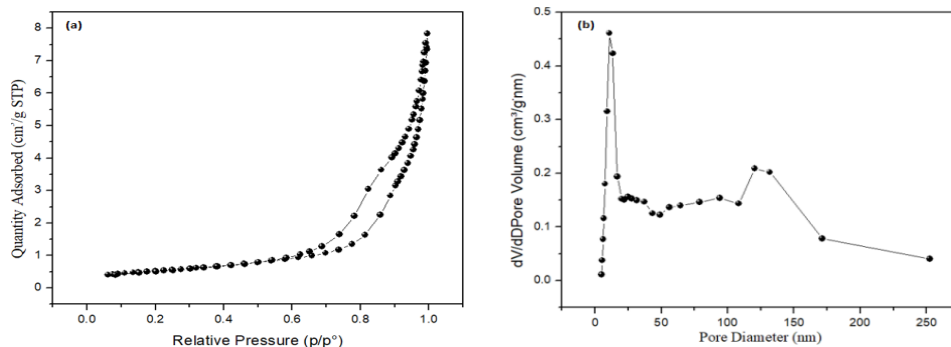


Fig.3. (a) Nitrogen adsorption-desorption isotherms; (b) pore size distribution of the MgOSeTe nanocomposites

Table 1. Summary report of BET surface area analysis of MgO_(86%) Se_(7%) Te_(7%).

Surface Area	
Single point surface area at $p/p^{\circ} = 0.298949197$:	41.0078 m ² /g
BET Surface Area:	42.0525 m ² /g
BJH Adsorption cumulative surface area of pores between 17.00 nm and 3,000.00 nm width:	46.266 m ² /g
Pore Volume	
BJH Desorption cumulative surface area of pores between 17.00 nm and 3,000.00 nm width:	0.265644 cm ³ /g
BJH Desorption cumulative volume of pores between 17.00 nm and 3,000.00 nm width:	0.298763 cm ³ /g
Pore Size	
BJH Adsorption average pore width (4V/A):	22.9665 nm
BJH Desorption average pore width (4V/A):	16.5065 nm
D-H Adsorption average pore width (4V/A):	23.3146 nm
D-H Desorption average pore width (4V/A):	16.3295 nm

3.4. Effect of initial dye concentration

Figure (4) exhibits the removal magnitude of MG dye via MgOSeTe nanopowder in an aqueous solution. From the figure, it can be observed that when the concentration increases, the removal rises too. The reason might be attributed to an increase in the driving force of the concentration gradient with the rise in the initial MG concentration [21]. As a result, the highest removal magnitude recorded was 99.98 %, and the lowest was 99.96 %. This means that the MgOSeTe nanocomposite has distinct properties in MG removal.

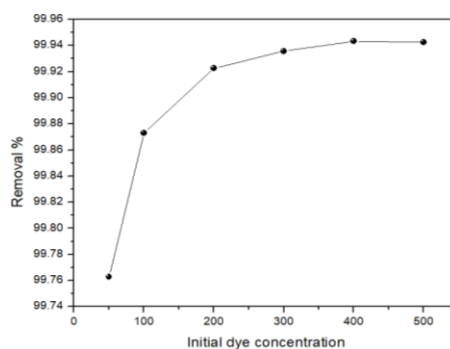


Fig. 4. Effect of initial dye concentration on removal efficiency.

3.5. Effect of contact time

Figure (5) demonstrates the dye removal magnitude versus contact times. The tests were conducted at several times (5, 10, 15, 20, 25, 30). The result showed that the removal of MG increases with time increase. Approximately 96 % of dye removal happened nearby 10 min. This is due to the availability of many active sites on the surface of the MgOSeTe nanocomposite [22]. The Adsorption equilibrium of the experiments was achieved in 20 min; at this point 96 % of the dye was removed. Thus, the fast time to remove the stain from water is 10 min.

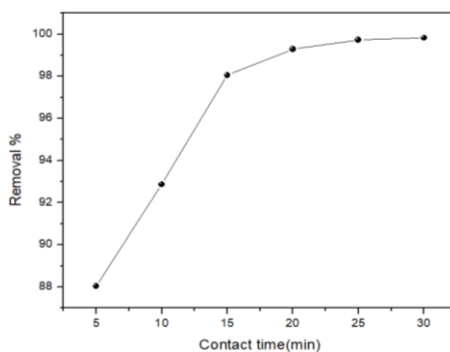


Fig. 5 Effect of contact time on removal efficiency.

3.6. Effect of pH on removal efficiency

Figure (6) displays the percentage removal of G dye through MgOSeTe nanocomposite in different pH (1,3,5,7,9,11). The test was done at 200-ppm MG dye with (0.071 g) of MgOSeTe for a 30 min equilibrium time. From the figure, it is seen that removal of dye increase with PH increases. This is due to the electrical attraction between the two surfaces of the negatively charged absorbent material and the positively charged dye molecules [23].

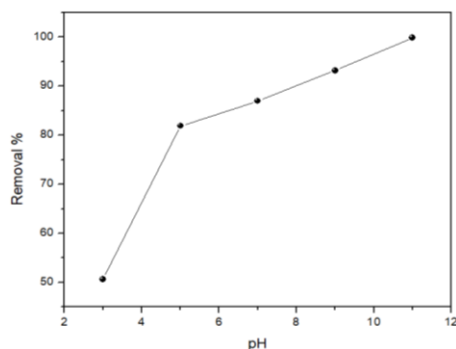


Fig. 6. Effect of pH on removal efficiency.

3.7. Adsorption isotherm

In this work, Langmuir and Freundlich isotherms have been implemented. Figures 7 and 8 display the linearized Langmuir adsorption and Freundlich isotherms for dye elimination by MgOSeTe nanocomposite. The Langmuir isotherms factors were estimated applying the least-squares method Table (2) shows the Langmuir and Freundlich isotherms factors for dye adsorption by MgOSeTe nanocomposite. From table (1), the Langmuir isotherm constant reported the value of (q_m) was determined to be 30.67 mg/g. Furthermore, the Langmuir isotherm constant can be described by the equilibrium factor (separation factor RL), a constant without dimensions as depicted in formula 9[24].

$$R_L = \frac{1}{1 + k_f \times C_0} \quad (9)$$

If the value of R_L ranged from 0 and 1, this indicates that the adsorption is suitable for all the initial dye concentrations. Furthermore, the value of the Freundlich isotherm constant (n) means the adsorption intensity, and the value of n was between 1 and 10; this confirms the favorable condition for the adsorption. The two models explain the correlation coefficient (R^2). From the obtained values of (R^2), the adsorption followed the Freundlich isotherms R^2 (0.9739). Although, various sorbents have been employed for MG dye elimination from the water system. Nevertheless, the MgOSeTe nanocomposite applied in this investigation have unique absorption capacity compared with other published adsorbents, as shown in table (4).

Table 2. Adsorption equilibrium constants for the dye removal by MgOSeTe nanocomposite.

Langmuir constants				Freundlich constants		
$q_m(\text{mg}\cdot\text{g}^{-1})$	$K_L(\text{l}\cdot\text{mg}^{-1})$	R_L	r^2	n	k_f	r^2
30.687	0.0238	0.1736	0.7968	0.7454	2.196	0.9739

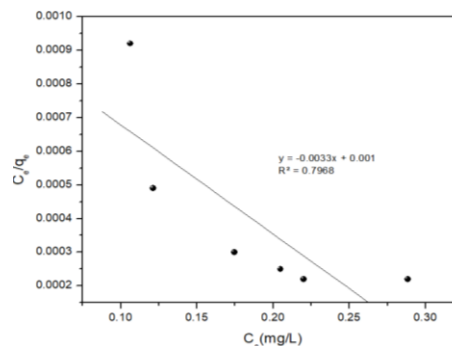


Fig. 7. Plot of linearized Langmuir adsorption isotherm.

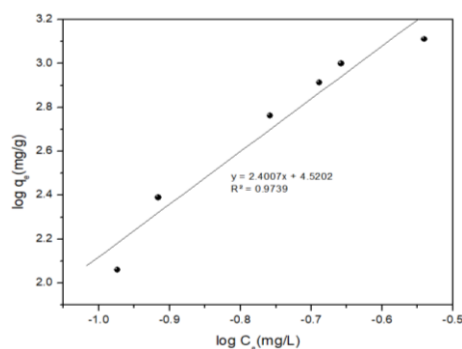


Fig. 8. Plot of linearized Freundlich adsorption isotherm.

Table 3. Comparison between the values of the adsorption capacity of MgOSeTe nanocomposite with other reported adsorbents.

Adsorbent	Adsorption capacity (mg/g)	Reference
ZnO/brick grain particles	35	[25]
Activated carbon	27.78	[26]
Commercial activated carbon	36.46	[27]
Commercial ZnO	29.6	[28]
MgO nanopowder	30.67	Current study

3.8. Adsorption kinetics

The kinetics of MG dye adsorption via MgOSeTe nanocomposite was investigated concerning various initial concentration. For estimating the Pseudo first order, the pseudo second order, were employed to fit the experimental data by using the linear regression analysis method. The parameters of this model are gathered in Table (4). High correlation coefficient magnitudes (R^2) indicate the suitability of the order of kinetic model. Figure (9) shows the pseudo-first-order kinetic model and figure (10) presents the pseudo-second-order kinetic model for MG dye removal by MgO nanopowder at room temperature. From the figures, the correlation coefficient (R^2) is high for the pseudo-second-order kinetic model than pseudo-first-order kinetic model. Therefore, the adsorption of MG dye via MgO nanopowder is obey the pseudo-second-order kinetic model. From the kinetic data information, the (q_e) value computed from the pseudo-first-order is less than the experimental value. Nevertheless, the calculated (q_e) value from the pseudo-second-order are almost closed to the experimental value

Table 4. Kinetic parameters for the dye adsorption by MgOSeTe nanocomposite.

$q_m(\text{exp})^a$ (mg.g^{-1})	First-order			Second-order		
	$k_1 \times 10^2$ (L.g^{-1})	$q_m(\text{cal})^b$ (mg.g^{-1})	r^2	k_2 ($\text{mg.g}^{-1} \cdot \text{L.g}^{-1}$)	$q_m(\text{cal})^b$ (mg.g^{-1})	r^2
58	0.164	16	0.987	0.0634	59.78	0.999

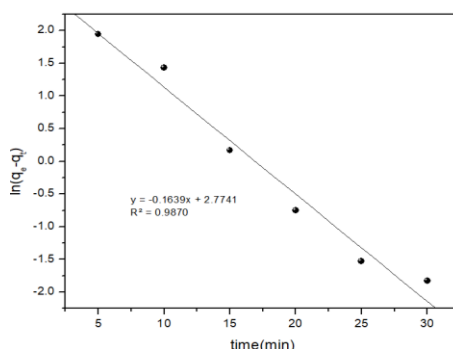


Fig. 9. Pseudo-first-order kinetic model for MG dye removal by MgOSeTe nanocomposite.

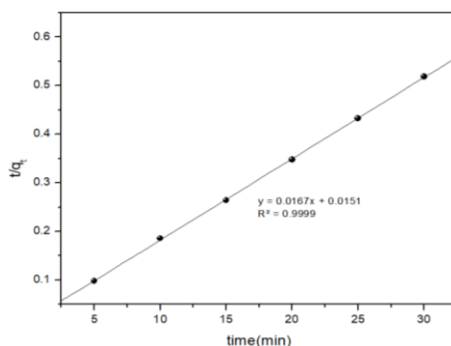


Fig. 10. Pseudo-second-order kinetic model for MG dye removal by MgOSeTe nanocomposite.

4. Conclusion

In summary, it can be concluded that the pyrolysis method is a good and easy way to produce MgOSeTe nanocomposite. The investigation has shown that MgOSeTe nanocomposite is powerful sorbent for malachite green remediation in water. The maximum capacity of MgOSeTe nanocomposite was 30.67 mg/g. Moreover, the adsorption of MG in water through MgOSeTe nanocomposite is followed the pseudo-second-order kinetic model.

Acknowledgements

This research was supported by the Deanship of Scientific Research, Imam Mohammad Ibn Saud Islamic University (IMSIU), Saudi Arabia, Grant No. (20-13-12-005). Hence, the authors would like to thank the Deanship of Scientific Research, Imam Mohammad Ibn Saud Islamic University (IMSIU), for their financial support.

References

- [1] O. Karlsson, J. Rocklöv, A. P. Lehoux, J. Bergquist, A. Rutgersson, M. J. Blunt, L. S. Birnbaum, *International Journal of Epidemiology* **50**(2), 378 (2021).
- [2] A. M. Elgarahy, K. Z. Elwakeel, S. H. Mohammad, G. A. Elshoubaky, *Cleaner Engineering and Technology*, 100209 (2021).
- [3] A. Tkaczyk, K. Mitrowska, A. Posyniak, *Science of The Total Environment* **717**, 137222 (2020).
- [4] I. Ihsanullah, A. Jamal, M. Ilyas, M. Zubair, G. Khan, M. A. Atieh, *Journal of Water Process Engineering* **38**, 101680 (2020).
- [5] A. A. Zewde, L. Zhang, Z. Li, E. A. Odey, *Reviews on environmental health* **34**(4), 365 (2019).
- [6] M. Ismail, K. Akhtar, M. I. Khan, T. Kamal, M. A. Khan, A. Asiri, S. B. Khan, *Current pharmaceutical design* **25**(34), 3645 (2019).
- [7] M. A. Islam, I. Ali, S. A. Karim, M. S. H. Firoz, A. N. Chowdhury, D. W. Morton, M. J. Angove, *Journal of Water Process Engineering* **32**, 100911 (2019).
- [8] D. S. Patil, S. M. Chavan, J. U. K. Oubagaranadin, *Journal of Environmental Chemical Engineering* **4**(1), 468 (2016).
- [9] S. Arslan, M. Eyvaz, E. Gürbulak, E. Yüksel, *Textile wastewater treatment*, 1 (2016).
- [10] M. Ismail, K. Akhtar, M. I. Khan, T. Kamal, M. A. Khan, A. Asiri, S. B. Khan, *Current pharmaceutical design* **25**(34), 3645 (2019).
- [11] K. Piaskowski, R. Świdarska-Dąbrowska, P. K. Zarzycki, *Journal of AOAC*

- International **101**(5), 1371 (2018).
- [12] J. B. Bhasarkar, B. A. Bhanvase, V. B. Pawade, Multifunctional Nanostructured Metal Oxides for Energy Harvesting and Storage Devices, 309 (2020), CRC Press.
- [13] M. A. M. Adnan, N. M. Julkapli, S. B. Abd Hamid, Reviews in Inorganic Chemistry **36**(2), 77 (2016).
- [14] S. M. Husnain, U. Asim, A. Yaqub, F. Shahzad, N. Abbas, New Journal of Chemistry **44**(16), 6096 (2020).
- [15] S. I. Siddiqui, O. Manzoor, M. Mohsin, S. A. Chaudhry, Environmental research **171**, 328019 (2020).
- [16] S. Yadav, A. Jain, P. Malhotra, Sustainable Materials and Technologies, e00315 (2021).
- [17] B. S. Marques, T. S. Frantz, T. R. S. A. C. Junior, L. A. de Almeida Pinto, G. L. Dotto, Environmental Science and Pollution Research **26**(28), 28584 (2019).
- [18] U. Habiba, T. A. Siddique, J. J. L. Lee, T. C. Joo, B. C. Ang, A. M. Afifi, Carbohydrate polymers **191**, 79 (2018).
- [19] R. Ezzati, Chemical Engineering Journal **392**, 123705 (2020).
- [20] Ş. Altındal, Ö. Sevgili, Y. Azizian-Kalandaragh, IEEE Transactions on Electron Devices **66**(7), 3103 (2019).
- [21] Z. Li, Y. Liu, H. Wang, C. J. Tsai, X. Yang, Y. Xing, P. A. Webley, Chemical Engineering Journal **353**, 858 (2018).
- [22] D. Y. Chung, P. P. Lopes, P. F. B. D. Martins, H. He, T. Kawaguchi, P. Zapol, N. M. Markovic, Nature Energy **5**(3), 222 (2020).
- [23] T. D. Pham, T. T. Pham, M. N. Phan, T. M. V. Ngo, C. M. Vu, Journal of Molecular Liquids **301**, 112456 (2020).
- [24] H. Idriss, A. Alakhras, Journal of Optoelectronic and Biomedical Materials **12**(4), 109 (2020).
- [25] P. Raizada, P. Singh, A. Kumar, G. Sharma, B. Pare, S. B. Jonnalagadda, P. Thakur, Applied Catalysis A: General **486**, 159 (2014).
- [26] T. Santhi, S. Manonmani, T. Smitha, Journal of hazardous materials **179**(1-3), 178 (2010).
- [27] I. D. Mall, V. C. Srivastava, N. K. Agarwal, I. M. Mishra, Colloids and Surfaces A: Physicochemical and Engineering Aspects **264**(1-3), 17 (2005).
- [28] J. Zhang, X. Yan, M. Hu, X. Hu, M. Zhou, Journal of Molecular Liquids **249**, 772 (2018).